NASA CONTRACTOR REPORT

NASA CR-1198

THE EFFECT OF THE CONVERGING FLOW FIELD OF A TANDEM-TEST-SECTION ON LONGITUDINAL STABILITY MEASUREMENTS

by Shojiro Shindo and Robert G. Joppa

Prepared by
UNIVERSITY OF WASHINGTON
Seattle, Wash.
for Langley Research Center

NATIONAL AERONAUTICS AND SPACE ADMINISTRATION • WASHINGTON, D. C. • OCTOBER 1968

THE EFFECT OF THE CONVERGING FLOW FIELD OF A TANDEM-TEST-SECTION ON LONGITUDINAL STABILITY MEASUREMENTS

By Shojiro Shindo and Robert G. Joppa

Prepared under NASA Grant NGR-48-002-010 by
UNIVERSITY OF WASHINGTON
Seattle, Wash.

for Langley Research Center

NATIONAL AERONAUTICS AND SPACE ADMINISTRATION

For sale by the Clearinghouse for Federal Scientific and Technical Information
Springfield, Virginia 22151 – CFSTI price $3.00

THE EFFECT OF THE CONVERGING FLOW FIELD OF A TANDEM-TEST-SECTION ON LONGITUDINAL STABILITY MEASUREMENTS

By Shojiro Shindo

and Robert G. Joppa

SUMMARY

Calculations of the internal flow in tandem-test-section wind tunnels have shown the presence of converging flow in the large test section portion between the two contracting sections.

Results of analytical and experimental work in a test section having length to height ratio of 3 show that the magnitude of the converging flow and its effect on longitudinal stability of a rigid rotor can be closely predicted. Maximum model sizes and satisfactory testing regions can be identified analytically. A prediction is made for two model sizes tested in a tunnel having length to height ratio of 1.

INTRODUCTION

A theory has been developed in Reference 1 to calculate the internal flow field of a square cross-section wind tunnel using a vortex ring method. This theory, when applied to a two contraction, two-test-section wind tunnel shows that the contracting

flow is not confined to the geometrically contracting region, but extends both upstream and downstream into the parallel wall test section regions for a distance about equal to the tunnel height. Thus, in the larger upstream test section a region of parallel flow would not be expected unless the length to height ratio is 2 or more. If the test section is shorter than that, or if the model is tested too near the ends, it would be in a region of converging flow.

If a rotor, for example, is placed in a converging flow field at an angle of attack, α , the trailing edge of the rotor would have a higher local angle of attack than the leading edge. This would cause the rotor to produce more nose down pitching moment than it would produce in a uniform parallel flow field at the same angle of attack. Furthermore, the amount of change in pitching moment due to the converging flow field is proportional to the rotor angle of attack and so the effect appears as an increase in the pitch stability. The same effect would be felt by any long model, such as a wing and tail. This study is intended to demonstrate that this effect is predictable.

The tunnel used for this study is a 1/8 scale model of the UWAL* 8 ft. by 12 ft. wind tunnel, modified by the addition of a V/STOL test section between the big end and the high speed test section. The V/STOL section is nearly square, has a length to height ratio of 3, is preceded by a bellmouth and contraction of 2.22, and followed by a contraction of 4.31 to the high speed

*University of Washington Aeronautical Laboratories

section. Reference 2 describes the model tunnel in more detail.

The method of calculating the internal flow field as presented in Reference 1 was used on this tunnel to calculate the extent and magnitude of the converging flow in the test section due to the contracting sections both upstream and downstream. The flow angles thus calculated were then used to predict the effects on thrust and pitching moment of a rotor at various longitudinal locations in the test section. These results are then compared with experiment.

SYMBOLS

a	Section lift curve slope, radians
a_o	Rotor coning angle, radians
A_0, A_1, A_2, A_3	Constants related to converging flow angle distribution
b	Number of blades per rotor
c	Blade section chord, ft.
C	Constant of integration
C_m	Pitching moment coefficient, $\frac{M}{\rho\pi(\Omega R)^2 R^3}$
D	Rotor diameter, ft.
h	Test section total height, ft.
K_1, K_2, K_3, K_4	Terms related to rotor pitching moment and thrust due to converging flow field
M	Rotor pitching moment, positive nose up, ft.-lb. unless otherwise noted

q	Tunnel dynamic pressure, psf
r	Radial distance to blade element, ft.
R	Blade radius, ft.
s	Disk area, sq. ft.
U_P	Component of resultant velocity parallel to the control axis at blade element, fps
U_T	Component of resultant velocity perpendicular to the control axis and to the blade span axis at blade element, fps
V	Tunnel center line velocity, fps
V'	Rate of change of induced velocity per rotor radius along longitudinal axis of rotor at $r = 0$, fps
V_o	Momentum theory value of rotor-induced velocity, $\frac{1/2\ C_T \Omega R}{\sqrt{\mu^2+\lambda^2}}$, fps
V_L	Local velocity at blade element, fps
x	Longitudinal distance from rotor hub centerline to blade element, ft.
X	Longitudinal distance measured from test section centerline when related to converging flow angle distribution, ft.
x_o	Longitudinal distance measured from test section centerline to rotor centerline, ft.
y	Vertical distance measured from test section centerline, positive down, ft.
α	Angle of attack, positive when shaft axis is inclined rearward, radians unless otherwise noted

θ	Blade section pitch angle; angle between line of zero lift of blade section and plane perpendicular to rotor shaft axis, radians
λ	Inflow ratio, $\frac{V \sin \alpha - V_o}{\Omega R}$
λ'	$\frac{V'}{\Omega R}$
μ	Tip speed ratio, $\frac{V \cos \alpha}{\Omega R}$
ρ	Mass density of air, slugs/cu. ft.
σ	Rotor solidity, $\frac{bc}{\pi R}$
Φ	Flow angle, radians
ψ	Blade azimuth angle measured from downwind position in direction of rotation, radians unless otherwise noted
Ω	Rotor angular velocity, radians/sec.

THEORY OF ROTOR THRUST AND PITCHING MOMENT IN A CONVERGING FLOW FIELD

The theory of Reference 1 was applied to the UWAL model tunnel to show the magnitude and extent of the converging flow field. Using the converging flow angle distribution thus calculated, the effect of such a flow field on the rotor thrust and pitching moment is analyzed.

The flow in the region around the longitudinal centerline of the tunnel can be described in terms of a centerline velocity vector which is coincident in direction with the tunnel centerline,

and a gradient of the flow inclination from the centerline taken in a direction normal to the centerline. Figure 1 shows a rotor in a flow field where the flow angle varies with height in the tunnel. The figure also shows a representative distribution of values of the flow angle along a vertical section measured from the tunnel centerline. This gradient, rate of change of flow inclination, $\frac{d\Phi}{d(y/h)}$, is nearly constant over the region which might be occupied by the model. The gradient varies along the length of the tunnel.

Values of this gradient along the length of the tunnel have been computed for the present example and are shown in Figure 2 along with a sketch showing the tunnel geometry. The longitudinal distribution is described by a third degree equation.

$$\frac{d\Phi}{d(y/h)} = A_3\left(\frac{x}{h}\right)^3 + A_2\left(\frac{x}{h}\right)^2 + A_1\left(\frac{x}{h}\right) + A_0 \qquad (1)$$

The constants A_n were chosen to give a fit within .04 of $\frac{d\Phi}{d(y/h)}$ for $-1.6 < x/h < 1.6$. The flow angle at a point in the tunnel is then

$$\Phi = \frac{d\Phi}{d(y/h)}\,(y/h) + C \qquad (2)$$

where C must be zero since the angle Φ is antisymmetric about the longitudinal axis and is zero on centerline $(y/h = 0)$.

Combining Equations (1) and (2), the following equation is obtained:

$$\Phi = \frac{y}{h}\left[A_3\left(\frac{X}{h}\right)^3 + A_2\left(\frac{X}{h}\right)^2 + A_1\left(\frac{X}{h}\right) + A_0\right] \qquad (3)$$

The angle Φ distribution described by Equation (3) is then converted into the rotor coordinate system by using the following equations.

$$\frac{X}{h} = \frac{x_o}{h} + \frac{x}{h}$$

$$y = r \sin \alpha \cos \psi$$

$$x = r \cos \alpha \cos \psi$$

where $x_{o/h}$ is the longitudinal location of the rotor centerline measured from the center of the straight portion of the test section. Then the flow angle at any point, r , on the rotor located downstream or upstream of the tunnel test section centerline is:

$$\Phi = \frac{r \sin \alpha \cos \psi}{h}\left[A_3\left(\frac{x_o}{h} + \frac{x}{h}\right)^3 + A_2\left(\frac{x_o}{h} + \frac{x}{h}\right)^2 + A_1\left(\frac{x_o}{h} + \frac{x}{h}\right) + A_0\right] \qquad (4)$$

The velocity components and angles (in their positive directions) at the blade element are shown in Figure 3, and the following equations were obtained:

$$U_T = \Omega r + \mu\Omega R \sin \psi - V \sin \alpha \tan \Phi \sin \psi \qquad (5)$$

$$U_p = \lambda\Omega R - \lambda'\Omega r \cos \psi + \mu\Omega R \tan \Phi \qquad (6)$$

The terms with tan Φ have been added to the basic velocity component equations to account for the converging flow field. It is assumed, for simplicity, that the longitudinal centerline velocity gradient due to the converging flow is negligible.

The thrust of a rotor is given by Reference 3.

$$T = \frac{b}{2\pi} \int_0^{2\pi} \int_0^R \frac{1}{2} \rho a (\theta U_T^2 + U_p U_T) c dr d\psi \qquad (7)$$

An expression for the thrust of a rotor in a converging flow field can be obtained by integrating the Equation (7) after the proper substitution of Equations (4), (5), and (6) by noting that the angle Φ is small, and assuming that the blade chord, pitch angle, and blade section lift curve slope are constant.

$$T = \frac{1}{2} \rho abc\Omega^2 R^3 \left[\frac{\theta}{3} + \frac{\theta\mu}{2} + \frac{\lambda}{2} - \frac{\theta\mu^2 \sin \alpha}{2} \left(\frac{R}{h}\right)^2 \{K_1\} + \frac{\mu \sin \alpha \cos \alpha}{4} \left(\frac{R}{h}\right)^4 \{K_2\} \right] \qquad (8)$$

where:

$$K_1 = A_3 \left[\frac{1}{2} \left(\frac{x_o}{h}\right)^2 + \frac{1}{20} \left(\frac{R \cos \alpha}{h}\right)^2 \right] + A_2 \left[\frac{1}{3} \left(\frac{x_o}{h}\right) \right] + \frac{A_1}{6}$$

$$K_2 = A_3\left[\frac{3}{2}\left(\frac{x_o}{h}\right)^2 + \frac{1}{4}\left(\frac{R\cos\alpha}{h}\right)^2\right] + A_2\left(\frac{x_o}{h}\right) + \frac{A_1}{2}$$

The last two terms in the large brackets of Equation (8) are the thrust increments due to the converging flow field.

The pitching moment of the rotor is according to Reference 4.

$$M = \frac{b}{2\pi}\int_0^{2\pi}\int_0^R -\frac{1}{2}\rho ac(\theta U_T^2 + U_p U_T) r\cos\psi d\psi dr \qquad (9)$$

Substituting Equations (4), (5), and (6) into (9), and performing the integration by assuming that the blade chord, pitch angle, and blade section lift curve slope are constant, the following equation can be obtained:

$$M = \frac{1}{4}\rho abc\Omega^2 R^4\left[\frac{\lambda'}{4} + \frac{\theta\mu V\sin^2\alpha}{2\Omega Rh}\{K_3\} - \frac{\mu R\sin\alpha}{4}\{K_4\}\right] \qquad (10)$$

where:

$$K_3 = A_3\left[\frac{1}{2}\left(\frac{x_o}{h}\right)^3 + \frac{3}{8}\left(\frac{x_o}{h}\right)\left(\frac{R\cos\alpha}{h}\right)^2\right] + A_2\left[\frac{1}{2}\left(\frac{x_o}{h}\right)^2 + \frac{1}{8}\left(\frac{R\cos\alpha}{h}\right)^2\right]$$

$$+ A_1\left[\frac{1}{2}\left(\frac{x_o}{h}\right)\right] + \frac{A_0}{2}$$

$$K_4 = A_3\left[\left(\frac{x_o}{h}\right)^3 + \frac{3}{2}\left(\frac{x_o}{h}\right)\left(\frac{R\cos\alpha}{h}\right)^2\right] + A_2\left[\left(\frac{x_o}{h}\right)^2 + \frac{1}{2}\left(\frac{R\cos\alpha}{h}\right)^2\right]$$

$$+ A_1\left(\frac{x_o}{h}\right) + A_0$$

The pitching moment shown by Equation (10) is identical to that of Equation (A14) of Reference 4 except that Equation (10) contains additional terms which are due to the converging flow field.

The rotor used in this study has highly twisted blades with variable chord. In integrating Equations (7) and (9), it was assumed that the blade chord, pitch angle, and the blade section lift curve slope were constant along the rotor radius. The values of the blade chord and section lift slope at .75 radius were used as representative of the real rotor. An effective blade pitch angle was selected which, when used to calculate the rotor thrust, gave good agreement with experimental values obtained at the center of the test section. The blade pitch angle thus selected was used to compute the rotor pitching moment at all longitudinal locations. The results obtained by these equations are discussed in the latter part of this paper.

EXPERIMENTAL STUDY

An experimental study to find the converging flow field effects predicted above was carried out using a rigid rotor in the UWAL 1/8 scale model tunnel previously described.

The rotor used is a rigid three bladed aluminum propeller with a diameter of 15 inches, which is half the height of the test section. The rotor was operated at 6000 rpm which resulted in a maximum tested tip speed ratio of .15 . The minimum tip speed ratio tested was .10 to avoid the adverse effect of near hover

condition which is described in Reference 5. The rotor is attached to a six component strain gage balance, and the entire rotor and balance assembly can be pitched about the rotor hub center. The rotor was tested at nine locations distributed along the longitudinal centerline of the tunnel. During these test runs the rotor lift, drag, side force, pitching moment, rolling moment and yawing moment were measured at angles of attack from $+5^{\circ}$ to -20° by 5° increments. The results of these tests show relative changes in the rotor stability at the different longitudinal stations tested and are presented in the following section of this paper.

RESULTS AND DISCUSSION

The rotor thrust changes with angle of attack at the middle of the test section and at the extreme upstream station tested, $x_{o/h} = -1.22$, are shown in Figure 4. The repeatability shown here proves that the converging flow field has no significant effect on the rotor thrust. The analytical study to find the thrust change due to the converging flow field by Equation (8) showed that the change at the most downstream station tested is less than one percent of the rotor thrust.

The rotor pitching moment was measured at nine longitudinal locations and was plotted against the rotor angle of attack. A typical pitching moment curve measured is shown in Figure 5. From these plots the slope of the pitching moment curve, $dM/d\alpha$, at each station was measured at the straight portion of the curve

between the angles of attack of -15° and 0° . The slope thus obtained was compared against that obtained at the middle of the test section using two different methods. One method shows the slope decrease in ratio form and the other shows the slope changes as the difference between the slope at the middle of the test section and at the other locations.

Figure 6a shows rotor stability changes at each location in a form of a ratio of the slope of the pitching moment curve at any location to that at the longitudinal centerline. Figure 6b shows the slope changes as differences in the rotor stability between the value at the center of the test section and at other locations. Figures 6a and 6b also show the rotor stability changes due to the converging flow field theoretically obtained by the method described in this paper. The excellent agreement in these figures shows that the rotor stability increase due to the converging flow field can be estimated by the method described herein.

The experimental and analytical work presented above were based on a wind tunnel having a length to height ratio of approximately 3 which is perhaps larger than most existing or proposed tunnels. A sample calculation was also made to show the effect discussed in this report for a wind tunnel with a length to height ratio of approximately 1, which corresponds to the shortest section that has been constructed. This sample calculation was made for two different rotors in the test section. The analytical results for the flow angles are shown in Figure 7 and the stability changes

are presented in Figures 8a and 8b. Figure 8a shows the stability change in a ratio form based on the stability of the rotor in a parallel flow field. Figure 8b shows the stability changes as differences in rotor stability in parallel or converging flow fields. Here the results are presented in coefficient form. The results shown in the figures indicate that a smaller rotor has a larger region in which the model could be tested without significantly affecting the measured stability. The large magnitude of $\left(\frac{dCm}{d\alpha}\right)_{X/h} \Big/ \left(\frac{dCm}{d\alpha}\right)_{\mathfrak{L}}$ for $D/h = 0.578$ rotor is due to the extremely small value of $dCm/d\alpha$ in the parallel flow field.

CONCLUDING REMARKS

Convergence of the flow in the V/STOL test section of a tandem-test-section wind tunnel is one of the factors that would limit the usable length of the test section. The effect of a converging flow field on a long model is to increase the longitudinal stability. The magnitude of the change in stability due to such a flow field can be approximately calculated for a rigid rotor by the method presented in this paper, using the converging flow angle distribution computed by the method presented in Reference 1. The ability to calculate such stability changes of course requires suitable background theory for the configuration. The state of such theory is not now adequate for many V/STOL configurations.

For the case studied here with a length to height ratio of 3 and rotor diameter to height ratio of .5, it was found that about one half the test section length in the middle of the test section had satisfactory flow with no significant effect on the model.

A sample calculation using a tunnel length to height ratio of 1 and rotor diameter to height ratio of .578 showed that about one fifth the test section length immediately upstream of the test section centerline had satisfactory flow with little effect on the rotor stability. The same tunnel with a rotor of diameter to height ratio .29 was found to have satisfactory flow for about one half the test section length, located mostly immediately upstream of the test section center.

It is concluded that, for a given model and cross section of the test section, the length of the test section required to obtain satisfactory flow with no significant effect on longitudinal stability can be calculated by the method presented in this paper.

REFERENCES

1. Robert G. Joppa and Victor M. Ganzer. An Aerodynamic Feasibility Study of Two-Test-Section Wind Tunnels for V/STOL Testing. Paper presented at AIAA Aerodynamic Testing Conference, March 1964.

2. Shojiro Shindo and Robert G. Joppa. An Experimental Investigation of Feasibility of a V/STOL Test Section in UWAL 8 x 12 Wind Tunnel by Using a 1/8 Scale Model of the Tunnel. UWAL Report No. 801, 1965.

3. Alfred Gessow and Garry C. Myers, Jr.. Aerodynamics of Helicopter . The MacMillan Company, New York, 1952, p. 189.

4. George E. Sweet. Static-Stability Measurements of a Stand-on Type Helicopter with Rigid Blades Including a Comparison with Theory. NASA TN D-189, 1960.

5. William H. Rae, Jr.. Limits on Minimum-Speed V/STOL Wind-Tunnel Tests. Journal of Aircraft, Vol. 4, No. 3, 1967.

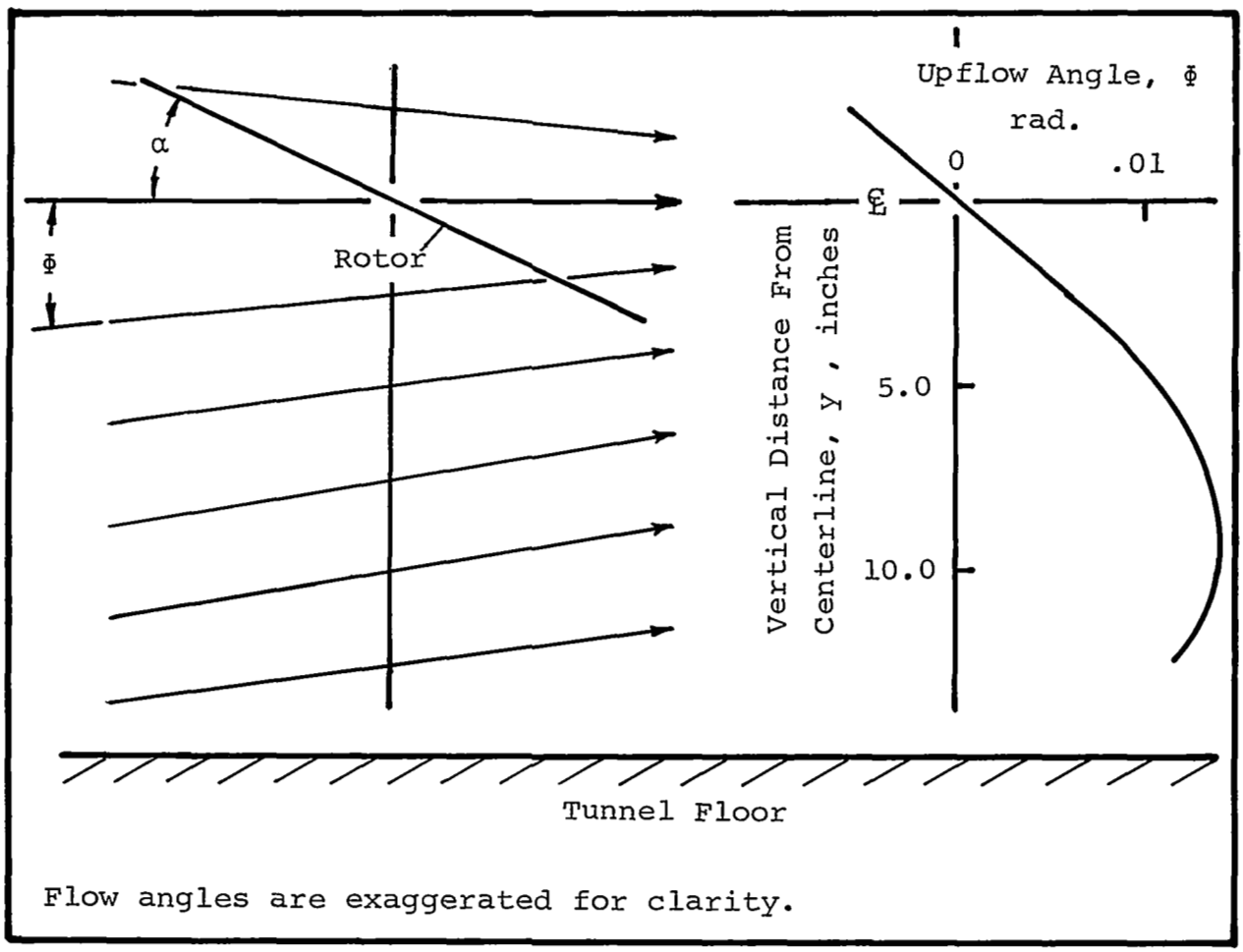

Figure 1 Flow Angle Distribution In Vertical Direction For Length To Height Ratio 3 Tunnel

Calculated At X/h = 1.25

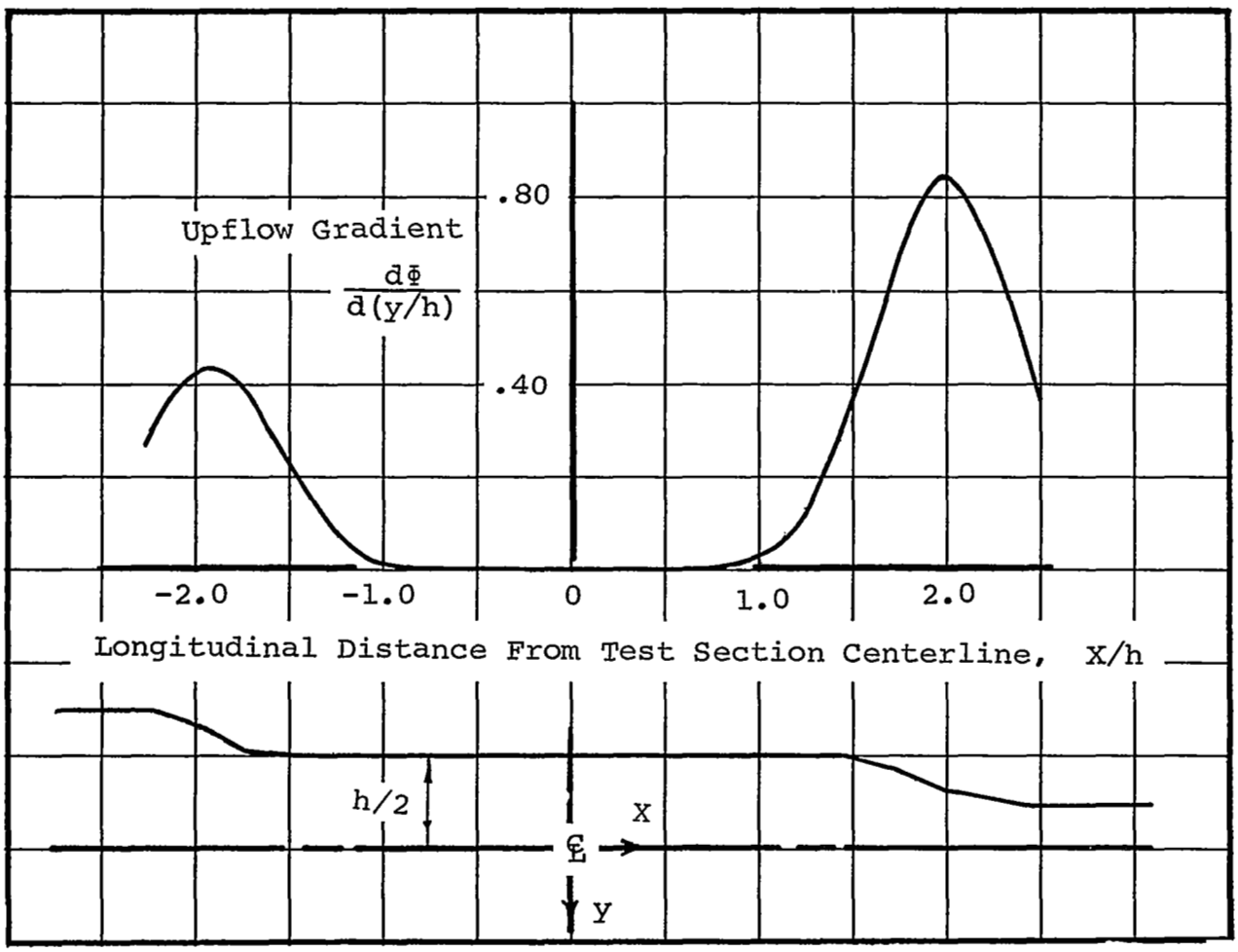

Figure 2 Upflow Distribution For
Length To Height Ratio 3 Tunnel

Calculated

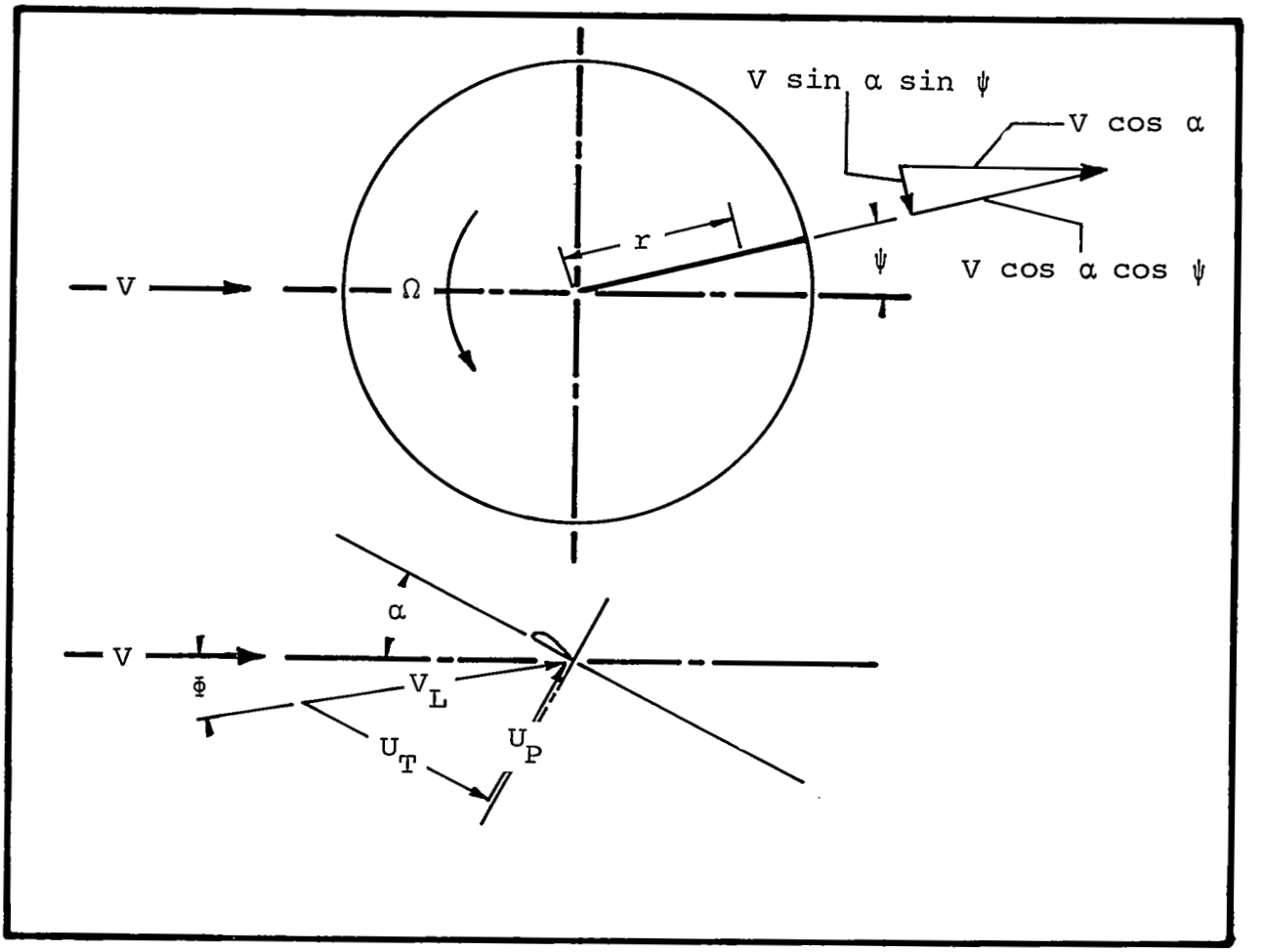

Figure 3 Velocity Components At Blade Element

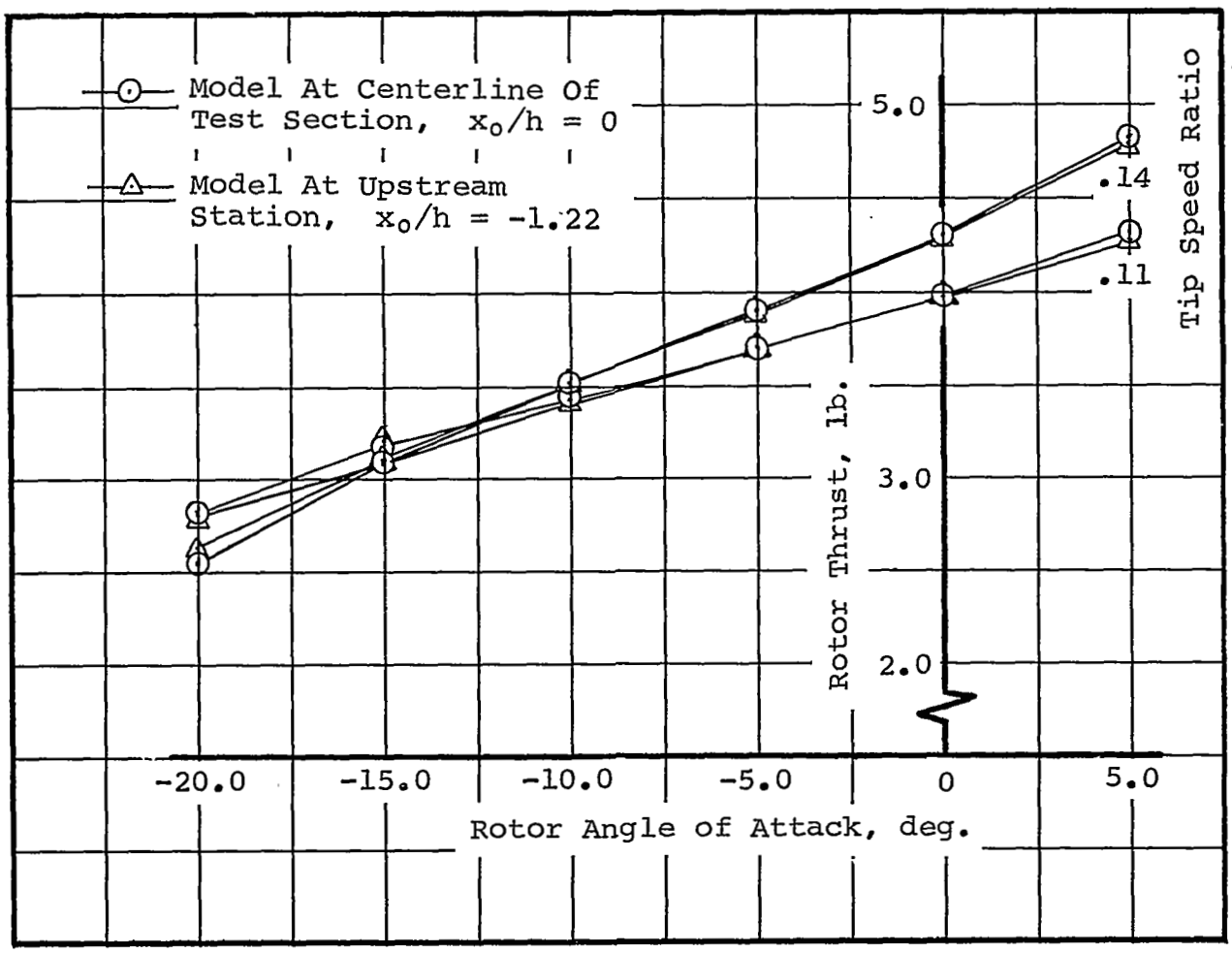

Figure 4 Effect Of Converging Flow Field On Rotor Thrust

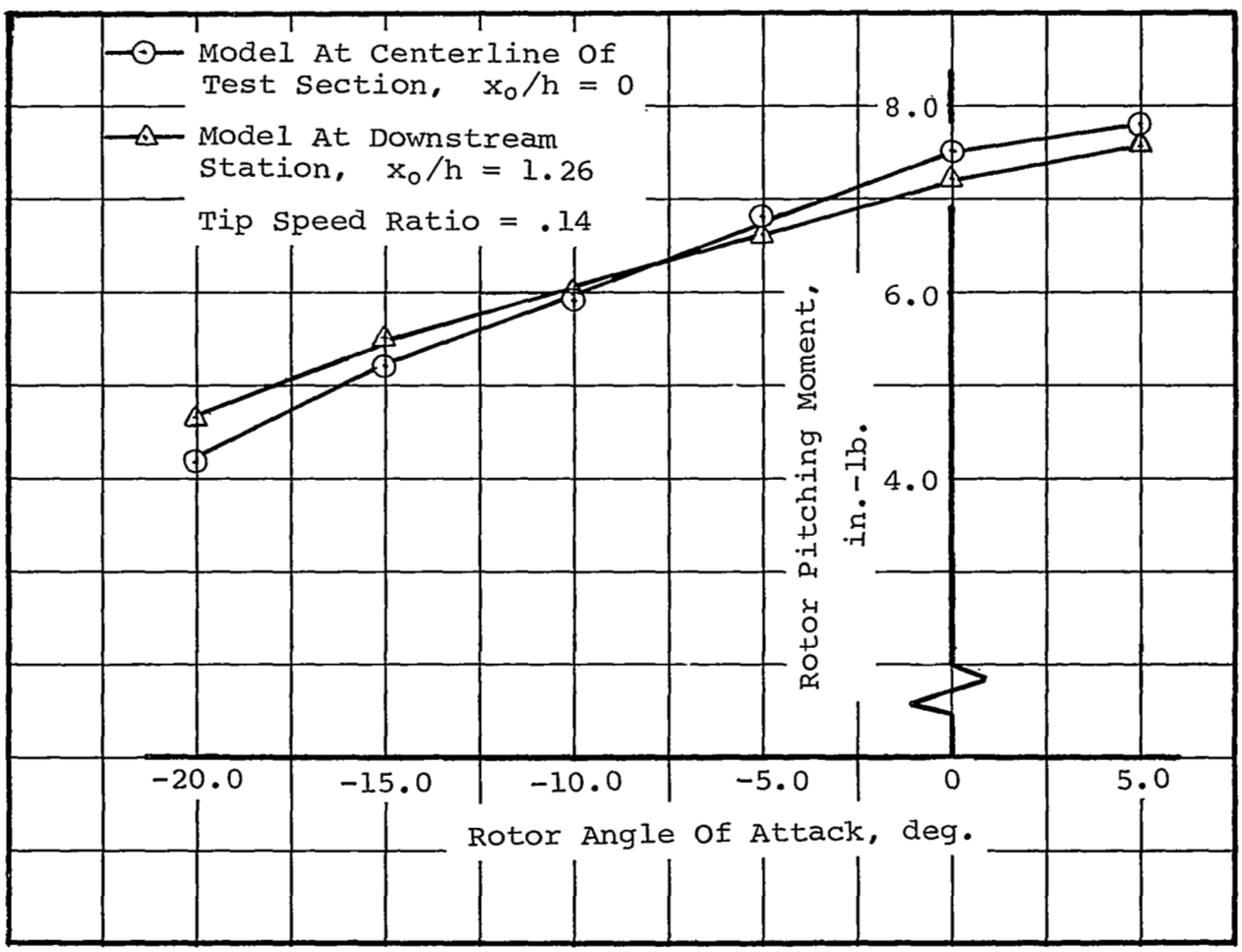

Figure 5 Effect Of Converging Flow Field On Rotor Pitching Moment

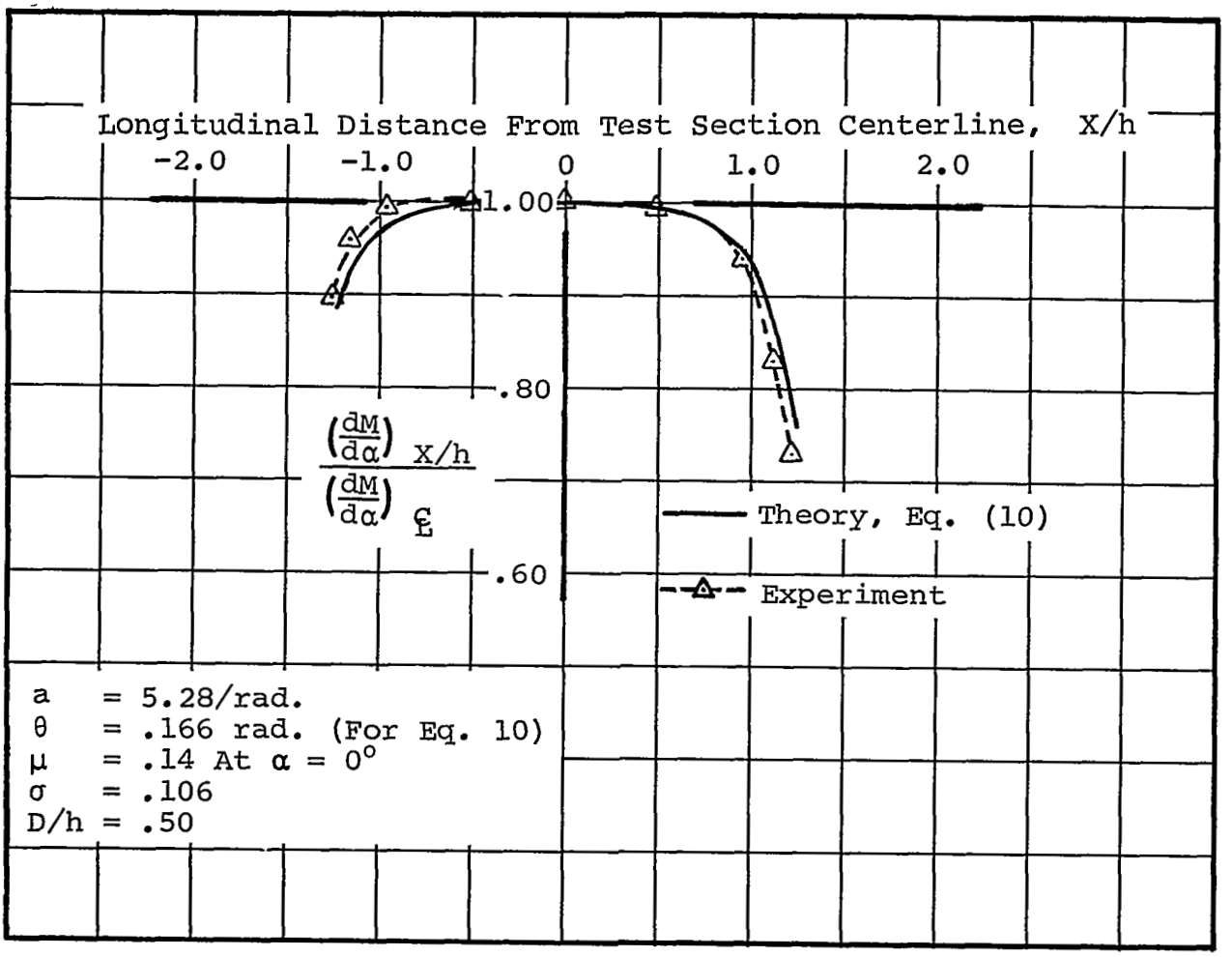

a) Stability Change Shown In A Form Of Ratio

Figure 6 Rotor Stability Change In Converging Flow Field For Length To Height Ratio 3 Tunnel

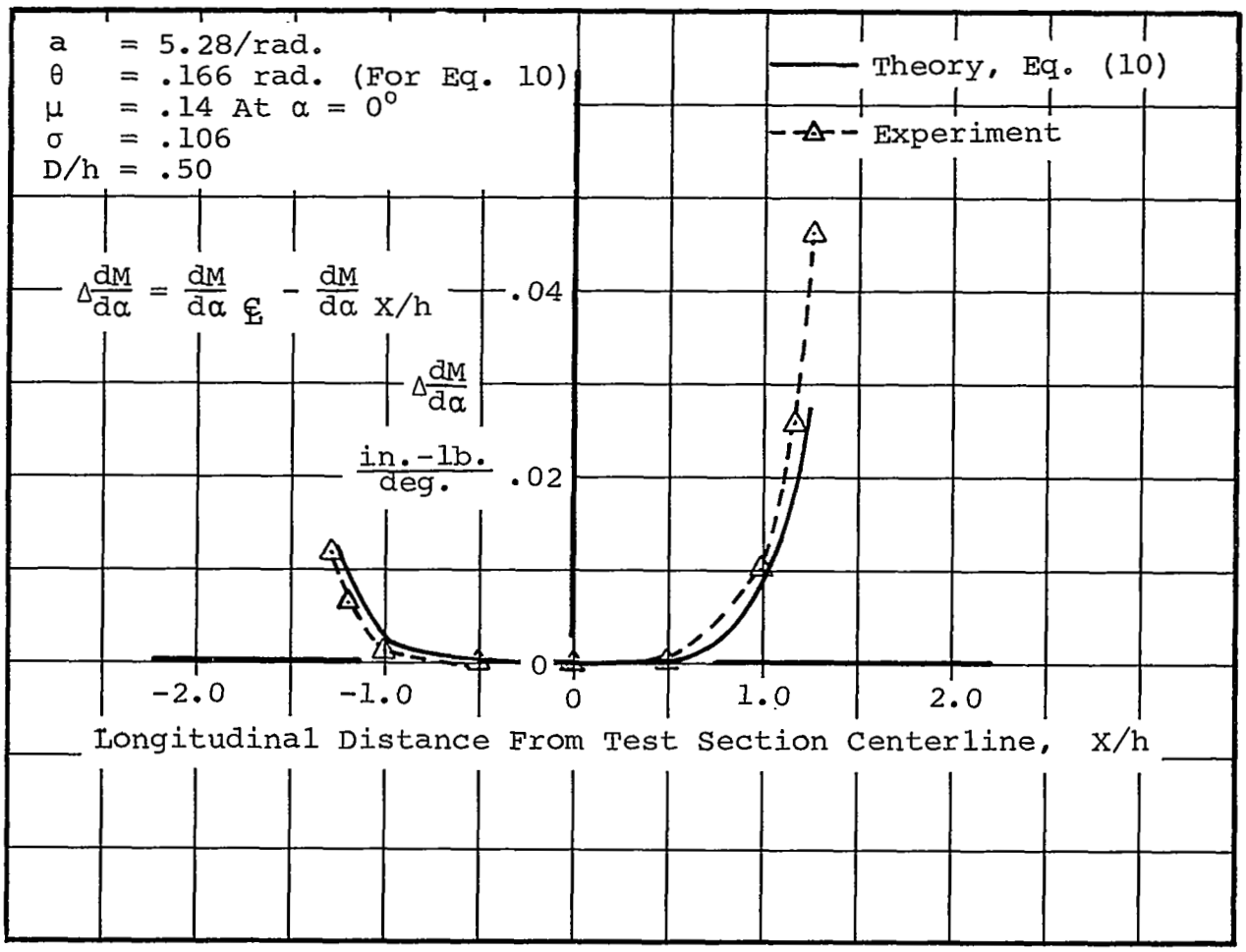

b) Stability Change Shown In A Form Of Difference

Figure 6 Concluded

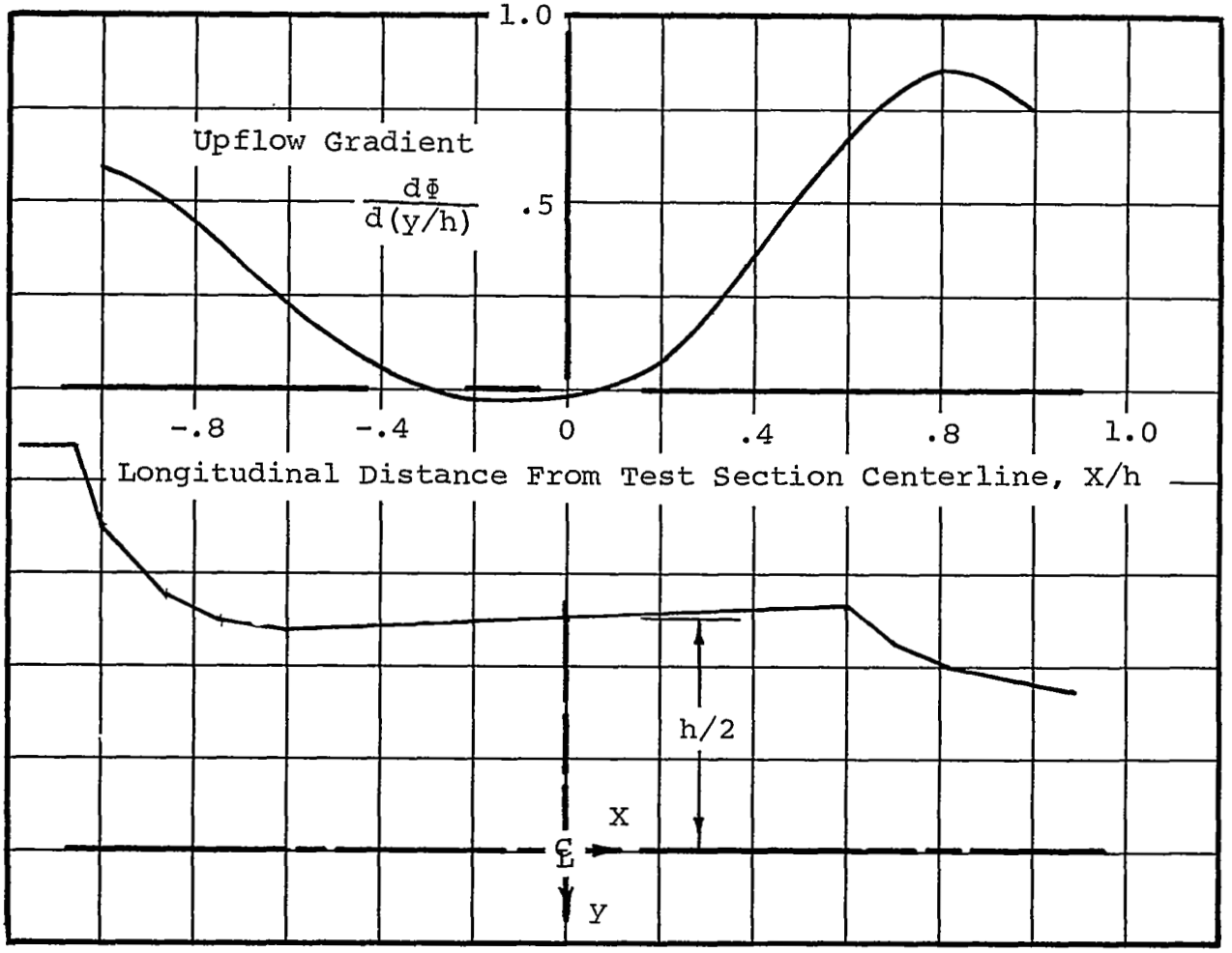

Figure 7 Upflow Distribution For Length To Height Ratio 1 Tunnel

Calculated

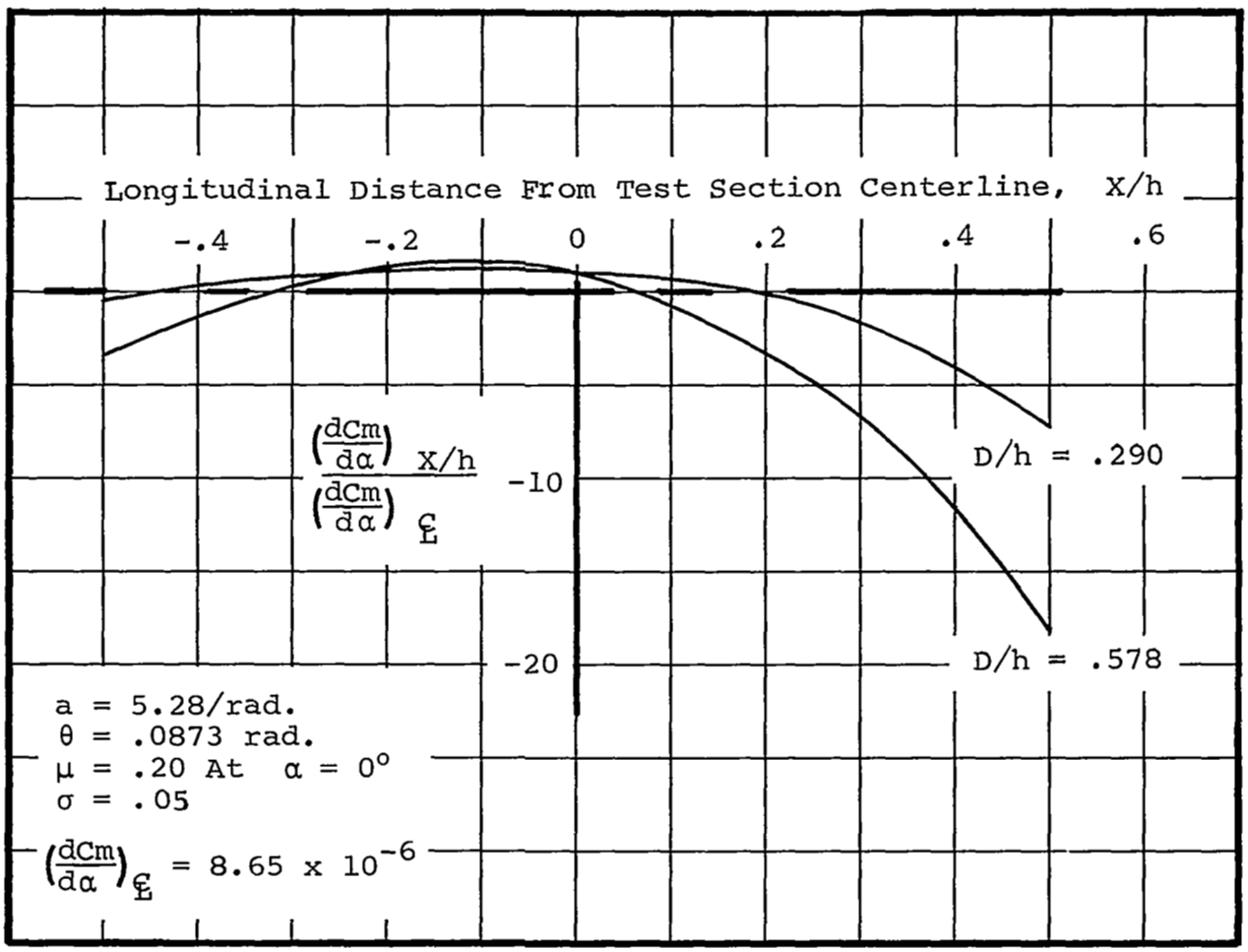

a) Stability Change Shown In A Form Of Ratio

Figure 8 Calculated Rotor Stability Change In Converging Flow Field For Length To Height Ratio 1 Tunnel

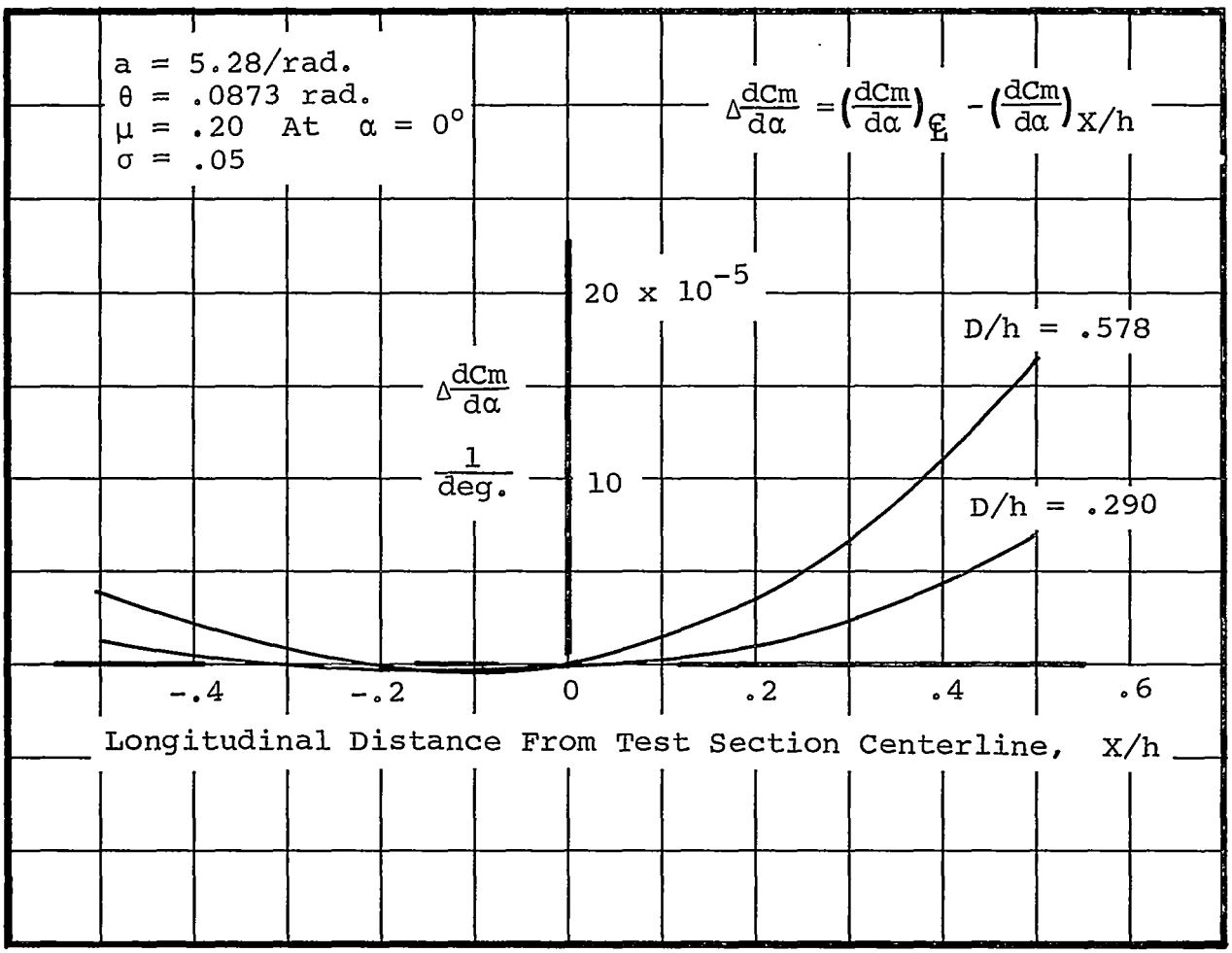

b) Stability Change Shown In A Form Of Difference

Figure 8 Concluded